SAPIENZA
UNIVERSITÀ DI ROMA

Fluid Structure Interaction Project Work Report

Fluid Structure Interaction

Prof.Alessio Castorrini

Laurea Magistrale di Meccanica and Master of Computational Mechanics - 1st year

Academic year 2023-2024

Fluid flow in a pipe-like structure

Author:
Antonin Maillard

Student number:
2161056

Tuesday 4th June, 2024

Contents

1 Introduction and problem overview

The study of Fluid-Structure Interactions (FSI) and flows within pipes encompasses a multifaceted domain critical to both fundamental fluid mechanics and numerous practical engineering applications. FSI involves the complex interplay between fluid flow and the structural dynamics of the boundaries containing or interacting with the fluid. This phenomenon is especially relevant in scenarios where the structural response significantly influences the flow characteristics and vice versa.
Fluid-structure interactions are omnipresent in various natural and engineered systems. For instance, blood flow in arteries or veins, wind loads on bridges and wind interactions with airfoils, and the motion of submarines in water all involve intricate FSI dynamics. In the context of pipe flows, understanding these interactions is paramount for the design and maintenance of numerous systems, including water distribution networks, oil and gas pipelines, and heat exchangers.
Pipes are ubiquitous in modern infrastructure, facilitating the transport of liquids and gases under a variety of conditions. The internal flow within these pipes can induce vibrations, stress, and deformation in the pipe walls, which in turn can affect the flow patterns. Such interactions are not merely a matter of academic interest; they have significant implications for the efficiency, safety, and longevity of piping systems.
This project work delves into the intricacies of fluid-structure interactions and flows in pipes, exploring both theoretical and practical aspects. The study covers several key areas: the theoretical mathematical foundations of fluid mechanics, structure mechanics, finite element analysis and their interactions, computational approaches for simulating these interactions such as finite elements methods (FEM), arbitrary simulations using real-world parameters and one real-world application and case study. Finally, this project work discusses the challenges and future directions in the field.
By addressing these areas, this project work aims to contribute to the body of knowledge in fluid mechanics and structural dynamics, providing valuable insights for both academic research and industrial practice. Through this work, we seek to pave the way for more resilient, efficient, and innovative engineering solutions in the context of fluid-structure interactions.

Initially, a framework is established to solve the problem. For this project work we consider a simple pipe with two right-angles (see the schematic of the pipe in Figure 1 (topview)). The pipe has a certain diameter which can be changed by the operator, it also has a thickness which can be a function of the diameter or manually set by the operator (see later for real-world case sudy). According to the geometry of the problem we can reduce the problem to a 2D problem, this allows for easier mathematical models and faster computations. In order for the solver and mesher to understand that we are simulating a 3D circular problem with a 2D model and that the "walls" of the pipe in 2D are actually the circular wall of the 3D pipe, we create thin "beams" linking the two walls (in the 2D model) along strategic points in the pipe. These beams will allow the walls to move as if they are paired one another, creating the motion of one single element juste like if it was a real circular pipe. This trick is an approximation and can induce small errors in the stresses at the strategic points where the beams link the two walls.
We make three important assumptions for the solid constituting the pipe: it is a homogeneous and isotropic material and its stress tensor varies linearly.
As for the fluid flow, we create an inlet at the bottom of the schematic and an outlet at the top. We also make assumptions for the fluid and fluid flow: the fluid is Newtonian, isotropic and considered continuous, the fluid flow is incompressible.

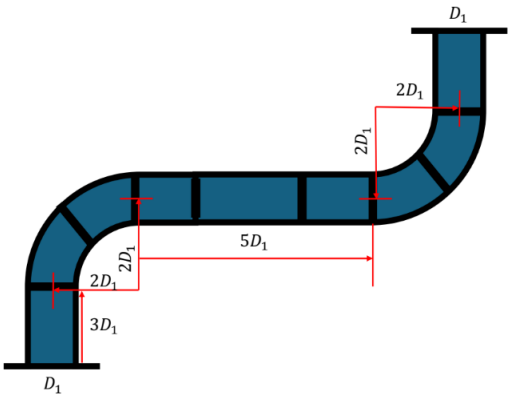

Figure 1: Simple schematic representation of the geometry of the pipe

2 Mathematical modelling

All mathematical, FEM discretization and algorithms derivations are taken from the course of Fluid Structure Interaction taught at Sapienza University of Rome by Prof. Alessio Castorrini & Prof. Franco Rispoli [1].

2.1 Fluid dynamics sub-system

2.1.1 Base method (for non-moving mesh)

In this section we will set up the governing equations of fluid mechanics for the fluid dynamics sub-system of our simulation. As said in the problem overview, we made 4 assumptions for the fluid and its flow which will be useful to simplify the Navier-Stokes (NS) equations. The assumption of a newtonian fluid is very important in order to apply the regular NS equations, the incompressibility of the flow is also a good assumption simplifying the equations because they mean a constant (with respect to time) density of the fluid. Finally, assuming an isotropic flow means that the density of the fluid does not depend on space.

The NS equations are as follows:

$$\text{Mass conservation: } \frac{\partial \rho}{\partial t} + \vec{\boldsymbol{\nabla}}(\rho \vec{u}) = 0 \tag{1}$$

$$\text{Momentum conservation: } \rho(\frac{\partial \vec{u}}{\partial t} + (\vec{u} \cdot \vec{\boldsymbol{\nabla}})\vec{u} + \vec{f}) + \vec{\boldsymbol{\nabla}} p - \mu \Delta \vec{u} = 0 \tag{2}$$

Using the Cauchy stress tensor and the linear strain-rate tensors:

$$\underline{\underline{\sigma}} = -p\underline{\underline{I}} + \mu \underline{\underline{\epsilon}}(\vec{u})$$

$$\underline{\underline{\epsilon}}(\vec{u}) = \frac{1}{2}(\underline{\underline{\boldsymbol{\nabla} u^T}} + \underline{\underline{\boldsymbol{\nabla} u}})$$

We can write:

$$\rho(\frac{\partial \vec{u}}{\partial t} + (\vec{u} \cdot \vec{\boldsymbol{\nabla}})\vec{u} + \vec{f}) - \boldsymbol{\nabla} \cdot \underline{\underline{\sigma}} = 0 \tag{3}$$

Thanks to the assumption of incompressible flow we can write:

$$\boldsymbol{\nabla} \cdot \vec{u} = 0 \tag{4}$$

Finally, we have the Navier-Stokes equations which follow:

$$\begin{cases} \rho(\frac{\partial \vec{u}}{\partial t} + (\vec{u} \cdot \vec{\boldsymbol{\nabla}})\vec{u} + \vec{f}) - \boldsymbol{\nabla} \cdot \underline{\underline{\sigma}} = 0 \\ \boldsymbol{\nabla} \cdot \vec{u} = 0 \end{cases} \tag{5}$$

Now that we have the Navier-Stokes equations, in order to implement them in a numerical scheme, the first step we have to make is define the weak form. This is called the Galerking Finite Element Method. The weak form is a weak hypothesis made from the equations to see if a particular trial and test function satisfies the governing equations.

In order to do that we have to define the set of infinite-dimensional trial functions that will model the velocity and the pressure solutions:

$$\begin{cases} S_u = \{\vec{u} | \vec{u}(x,t) \in H^1(\Omega_t), u_i = g_i \quad \text{on} \quad (\Gamma_t)_{gi}\} \\ S_p = \{p | p(\vec{x}) \in L^2(\Omega_t), \int_{\Omega_t} p d\Omega = 0 \quad \text{if} \quad \Gamma_t = (\Gamma_t)_{gi}\} \end{cases} \tag{6}$$

$L^2(\Omega_t)$ and $H^1(\Omega_t)$ are the spaces of scalar- and vector-valued functions square-integrable and with square-integrable derivatives on Ω_t. S_u satisfies the boundary conditions of the fluid mechanics.
Now we will define the set of test functions that will model the velocity and the pressure that will be tested to see if they can match the trial (solutions) functions defined just before:

$$\begin{cases} V_u = \{\vec{w} | \vec{w}(x,t) \in H_0^1(\Omega_t), w_i = 0 \quad \text{on} \quad (\Gamma_t)_{gi}\} \\ V_p = \{q | q(\vec{x}) \in L^2(\Omega_t), \int_{\Omega_t} q d\Omega = 0 \quad \text{if} \quad \Gamma_t = (\Gamma_t)_{gi}\} \end{cases} \tag{7}$$

$L^2(\Omega_t)$ and $H_0^1(\Omega_t)$ are the same spaces as defined before. Now what is left to do is follow certain steps to get to the weak formulation.

The first 3 steps are:

1. Multiply the equations by their corresponding test functions.
2. Integrate over the domain Ω_t.
3. Add the equations together.

After doing these 3 steps we get:

$$\int_{\Omega_t} \vec{w} \cdot \rho(\frac{\partial \vec{u}}{\partial t} + (\vec{u} \cdot \vec{\boldsymbol{\nabla}})\vec{u} - \vec{f})d\Omega - \int_{\Omega_t} \vec{w} \cdot (\boldsymbol{\nabla} \cdot \underline{\underline{\sigma}}(\vec{u}, p))d\Omega + \int_{\Omega_t} q\boldsymbol{\nabla} \cdot \vec{u}d\Omega = 0 \tag{8}$$

Now we need to integrate by parts the Cauchy stress term as it is the highest derivative.
Recalling that $\underline{\underline{\sigma}} = \underline{\underline{\sigma}}^T$ we find $\underline{\underline{\boldsymbol{\nabla}}}\vec{w} : \underline{\underline{\sigma}} = \underline{\underline{\epsilon}}(\vec{w}) : \underline{\underline{\sigma}}$
We get:

$$-\int_{\Omega_t} \vec{w} \cdot (\boldsymbol{\nabla} \cdot \underline{\underline{\sigma}}(\vec{u}, p))d\Omega = \int_{\Omega_t} \underline{\underline{\epsilon}}(\vec{w}) : \underline{\underline{\sigma}}(\vec{u}, p)d\Omega - \int_{(\Gamma_t)_h} \vec{w} \cdot \underline{\underline{\sigma}}(\vec{u}, p)\vec{n}d\Gamma$$

$\underline{\underline{\sigma}}(\vec{u}, p)\vec{n}$ is the traction vector and has a prescribed value on $(\Gamma_t)_h$ thanks to boundary conditions, meaning we can replace it with that value. We will call the latter $\vec{h}$ giving:

$$-\int_{\Omega_t} \vec{w} \cdot (\boldsymbol{\nabla} \cdot \underline{\underline{\sigma}}(\vec{u}, p))d\Omega = \int_{\Omega_t} \underline{\underline{\epsilon}}(\vec{w}) : \underline{\underline{\sigma}}(\vec{u}, p)d\Omega - \int_{(\Gamma_t)_h} \vec{w} \cdot \vec{h}d\Gamma$$

But recalling the definition of the set of test functions $\vec{w}(x, t) = 0$ on $(\Gamma_t)_h$, we get:

$$-\int_{\Omega_t} \vec{w} \cdot (\boldsymbol{\nabla} \cdot \underline{\underline{\sigma}}(\vec{u}, p))d\Omega = \int_{\Omega_t} \underline{\underline{\epsilon}}(\vec{w}) : \underline{\underline{\sigma}}(\vec{u}, p)d\Omega \tag{9}$$

Substituting (9) inside (8) will give the weak form of the Navier-Stokes equations for incompressible flows:
Find $\vec{u} \in S_u$ and $p \in S_p$ such that $\forall \vec{w} \in V_u$ and $\forall q \in V_p$:

$$\int_{\Omega_t} \vec{w} \cdot \rho(\frac{\partial \vec{u}}{\partial t} + (\vec{u} \cdot \vec{\boldsymbol{\nabla}})\vec{u} - \vec{f})d\Omega + \int_{\Omega_t} \underline{\underline{\epsilon}}(\vec{w}) : \underline{\underline{\sigma}}(\vec{u}, p)d\Omega + \int_{\Omega_t} q\boldsymbol{\nabla} \cdot \vec{u}d\Omega = 0$$

The last step to define the mathematical model of the fluid dynamics sub-system is to discretize the weak form of the Navier-Stokes equations.
The discretized variables are written as follows: $\vec{u}^h$, p^h, $\vec{w}^h$, q^h. We get:

$$\int_{\Omega_t} \vec{w}^h \cdot \rho(\frac{\partial \vec{u}^h}{\partial t} + (\vec{u}^h \cdot \vec{\boldsymbol{\nabla}})\vec{u}^h - \vec{f})d\Omega + \int_{\Omega_t} \underline{\underline{\epsilon}}(\vec{w}^h) : \underline{\underline{\sigma}}(\vec{u}^h, p^h)d\Omega + \int_{\Omega_t} q^h\boldsymbol{\nabla} \cdot \vec{u}^h d\Omega = 0$$

Now we need to define a discretization scheme by defining the unknown fields in terms of their finite element expansions:

$$\vec{u}^h = \sum_j \vec{u}_j\phi_j, \quad p^h = \sum_j p_j\psi_j$$

Where ϕ_j and ψ_j are the shape functions respectively associated to $\vec{u}^h$ and p_j.
The Galerkin method states that the tests functions are equal to the shape functions:

$$\vec{w}^h = \phi_i, \quad q^h = \psi_i$$

Substituting these expressions into the weark form found before we get the following terms:

Time Derivative Term:

$$\int_{\Omega_t} \vec{w}^h \cdot \rho\frac{\partial \vec{u}^h}{\partial t}\, d\Omega = \int_{\Omega_t} \phi_i \cdot \rho\frac{\partial}{\partial t}\left(\sum_j \vec{u}_j\phi_j\right) d\Omega = \sum_j \frac{d\vec{u}_j}{dt} \int_{\Omega_t} \rho\phi_i\phi_j\, d\Omega$$

Convection Term:

$$\int_{\Omega_t} \vec{w}^h \cdot \rho(\vec{u}^h \cdot \nabla)\vec{u}^h\, d\Omega = \int_{\Omega_t} \phi_i \cdot \rho\left(\left(\sum_k \vec{u}_k\phi_k\right) \cdot \nabla\right)\left(\sum_j \vec{u}_j\phi_j\right)\, d\Omega = \sum_{k,j} \vec{u}_k\vec{u}_j \int_{\Omega_t} \rho(\phi_i \cdot (\phi_k\nabla\phi_j))\, d\Omega$$

Body Force Term:

$$\int_{\Omega_t} \vec{w}^h \cdot \rho \vec{f}\, d\Omega = \int_{\Omega_t} \phi_i \cdot \rho \vec{f}\, d\Omega$$

Viscous Stress Term:

$$\int_{\Omega_t} \underline{\underline{\epsilon}}(\vec{w}^h) : \underline{\underline{\sigma}}(\vec{u}^h, p^h)\, d\Omega = \int_{\Omega_t} \nabla\phi_i : \underline{\underline{\sigma}} \left(\sum_j \vec{u}_j \phi_j, \sum_j p_j \psi_j \right) d\Omega$$

Divergence Term:

$$\int_{\Omega_t} q^h \nabla \cdot \vec{u}^h\, d\Omega = \int_{\Omega_t} \psi_i \nabla \cdot \left(\sum_j \vec{u}_j \phi_j \right) d\Omega = \sum_j \vec{u}_j \int_{\Omega_t} \psi_i \nabla \cdot \phi_j\, d\Omega$$

Adding all the terms together we get the following summation:

$$\sum_j \left[\int_{\Omega_t} \phi_i \cdot \rho \frac{d\vec{u}_j}{dt} \phi_j\, d\Omega + \int_{\Omega_t} \phi_i \cdot \rho(\vec{u}^h \cdot \nabla)\vec{u}_j \phi_j\, d\Omega + \int_{\Omega_t} \nabla\phi_i : \underline{\underline{\sigma}}(\vec{u}_j, p_j)\, d\Omega \right] = \int_{\Omega_t} \phi_i \cdot \rho \vec{f}\, d\Omega$$

Where the sum runs over the nodes of the finite element mesh.
In order to get rid of the integrals and have a fully numerically solvable expression, we will make use of the Gauss quadrature:

$$\int_{\Omega_t} f(\vec{x}) d\Omega \approx \sum_{i=1}^{N} w_i f(\vec{x}_i)$$

We finally get the following expression:

$$\sum_{i=1}^{n}\sum_{j=1}^{m} \left[w_i \rho \left(\frac{\partial \left(\sum_{i=1}^{n} \phi_i \vec{u}_i\right)}{\partial t} + \left(\left(\sum_{i=1}^{n} \phi_i \vec{u}_i \right) \cdot \nabla \right) \left(\sum_{i=1}^{n} \phi_i \vec{u}_i \right) - \vec{f} \right) \right.$$
$$\left. + w_i \underline{\underline{\epsilon}} \left(\sum_{i=1}^{n} \phi_i \vec{u}_i, \sum_{j=1}^{m} \psi_j p_j \right) : \underline{\underline{\sigma}}(\vec{u}_i, p_j) + w_i q^h \nabla \cdot \left(\sum_{i=1}^{n} \phi_i \vec{u}_i \right) \right] = 0$$

The last step is what the solver will essentially do in the end: solve $\underline{\underline{K}}\underline{U} = \underline{U}$
Where the displacement vector ($\underline{U}$) is the unknown we are looking for. The stiffness matrix ($\underline{\underline{K}}$) and the force vector ($\underline{\mathrm{F}}$) depend on the problem we are trying to solve, the boundary conditions, the geometry of the problem, the material properties and the external force.

2.1.2 Advanced method (for moving-meshes)

We have seen the base method for obtaining the governing equations and the weak formulation of a simple fluid dynamics problem. Unfortunately, this method is only for non-moving meshes where as our problem requires a moving mesh. Fortunately, this knowledge will be useful to derive another method for obtaining the weak formulation of governing equations of fluid dynamics for moving meshes.
We will use the Arbitrary Lagrangian-Eulerian Method (ALE). This method allows the computational system to not be a priori fixed in space and not fully attached to material.
To derive the ALE formulation we will first set the fluid spatial domain at any time:

$$\Omega_t = \{\vec{x} | \vec{x} = \vec{\phi}(\hat{\vec{x}}, t), \forall \hat{\vec{x}} \in \hat{\Omega}, t \in (0, T)\}$$

$\vec{\phi}(\hat{\vec{x}}, t)$ is the displacement maping and is defined as follows:

$$\vec{\phi}(\hat{\vec{x}}, t) = \hat{\vec{x}} + \vec{y}(\hat{\vec{x}}, t)$$

Where $\vec{y}$ is the displacement of the points of the fluid domain. Meaning we can define a subsequent flui ddomain velocity as follows:

$$\vec{\hat{u}} = \frac{\partial \vec{\hat{y}}}{\partial t} \quad \textbf{derivative taken with respect to the frame of reference}$$

Since we have defined a displacement field, we can define a deformation gradient and the Jacobian of the transformation subsequent to the fluid domain motion:

$$\underline{\underline{\hat{F}}} = \frac{\partial \vec{x}}{\partial \vec{\hat{x}}} = \underline{\underline{I}} + \frac{\partial \vec{\hat{y}}}{\partial \vec{\hat{x}}} \quad \hat{J} = \det \underline{\underline{\hat{F}}}$$

Now let's derive the ALE formulation of NS momentum equation in conservative form integrated over the moving flui ddomain:

Momentum equation in conservative form:

$$\int_{\Omega_t} \frac{\partial \rho \vec{u}}{\partial t} d\Omega + \int_{\Omega_t} \vec{\boldsymbol{\nabla}}(\rho \vec{u} \otimes \vec{u}) - \rho \vec{f} - \vec{\boldsymbol{\nabla}} \underline{\underline{\sigma}} d\Omega = 0 \tag{10}$$

Now let's recall the Reynold's transport theorem:

$$\left.\frac{d}{dt}\right|_{\hat{x}} \int_{\Omega_t} a d\Omega = \int_{\Omega_t} \left.\frac{\partial a}{\partial t}\right|_{\hat{x}} d\Omega - \int_{\Gamma_t} a(\vec{\hat{u}} \cdot \vec{n}) d\Gamma$$

And the Gauss divergence theorem:

$$\int_{\partial U} \vec{u} \cdot \vec{n} dS = \int_U \mathbf{div}(\vec{u}) dx$$

Combining both theorems we get:

$$\left.\frac{d}{dt}\right|_{\hat{x}} \int_{\Omega_t} \rho \vec{u} d\Omega = \int_{\Omega_t} \left.\frac{\partial \rho \vec{u}}{\partial t}\right|_{\hat{x}} d\Omega + \int_{\Omega_t} \vec{\boldsymbol{\nabla}}(\rho \vec{u} \otimes \vec{\hat{u}}) d\Omega \tag{11}$$

Substituting (11) in (10) and simplifying we get:

$$\left.\frac{d}{dt}\right|_{\hat{x}} \int_{\Omega_t} \rho \vec{u} d\Omega + \int_{\Omega_t} \vec{\boldsymbol{\nabla}}(\rho \vec{u} \otimes (\vec{u} - \vec{\hat{u}})) - \rho \vec{f} - \vec{\boldsymbol{\nabla}} \underline{\underline{\sigma}} d\Omega = 0$$

Now using the definition of the Jacobian and $\vec{\hat{F}}$ to pass from the current to the reference domain, where $\hat{J} = \frac{d\Omega}{d\hat{\Omega}}$ we obtain:

$$\left.\frac{d}{dt}\right|_{\hat{x}} \int_{\hat{\Omega}} \underline{\hat{F}}^{-1} \rho \vec{u} \hat{J} d\Omega + \int_{\hat{\Omega}} \underline{\hat{F}}^{-1} (\vec{\boldsymbol{\nabla}}(\rho \vec{u} \otimes (\vec{u} - \vec{\hat{u}})) - \rho \vec{f} - \vec{\boldsymbol{\nabla}} \underline{\underline{\sigma}}) \hat{J} d\Omega = 0$$

Since $\hat{\Omega}$ is the reference fluid domain, it doesn't move, thus, doesn't depend on time. Meaning that we get:

$$\int_{\hat{\Omega}} \frac{d}{dt} (\underline{\hat{F}}^{-1} \rho \vec{u} \hat{J}) d\Omega + \int_{\hat{\Omega}} \underline{\hat{F}}^{-1} (\vec{\boldsymbol{\nabla}}(\rho \vec{u} \otimes (\vec{u} - \vec{\hat{u}})) - \rho \vec{f} - \vec{\boldsymbol{\nabla}} \underline{\underline{\sigma}}) \hat{J} d\Omega = 0$$

Finally, performing the inverse transformation to go back to the current (that has moved) fluid domain and assuming an arbitrary volume in order to drop the integral we get the final expression:

$$\frac{1}{\hat{J}} \frac{d}{dt} (\rho \vec{u} \hat{J}) + \vec{\boldsymbol{\nabla}}(\rho \vec{u} \otimes (\vec{u} - \vec{\hat{u}})) - \rho \vec{f} - \vec{\boldsymbol{\nabla}} \underline{\underline{\sigma}} = 0 \tag{12}$$

Now all there is to do is find the weak form of this equation and use to find the Finite Element Method (FEM) form of the weak form. We will talk about the latter later in the report. Let's apply the same method for finding the weak form of the Navier-Stokes equations for non-moving meshes to equation (12) so that we get the following weak form:

$$\text{Find} \quad \vec{u}^h \in S_u^h, p^h \in S_p^h, \vec{y}^h \in S_y, \quad \text{such that} \quad \forall \vec{w}_1^h \in V_u^h, q^h \in V_p^h, \forall \vec{w}_2^h \in V_y^h$$

ALE weak form of Navier-Stokes equations for incompressible flows:

$$\begin{aligned} &\int_{(\Omega_1)_t} \vec{w}_1^h \cdot \rho \left(\left.\frac{\partial \vec{u}^h}{\partial t}\right|_{\hat{x}} + (\vec{u}^h - \vec{\hat{u}}^h) \cdot \nabla \vec{u}^h - \vec{f}^h \right) d\Omega \\ &+ \int_{(\Omega_1)_t} \boldsymbol{\epsilon}(\vec{w}_1^h) : \boldsymbol{\sigma}_1 \, d\Omega + \int_{(\Omega_1)_t} q_1^h \nabla \cdot \vec{u}^h \, d\Omega - \int_{\Gamma_{1E}} \vec{w}_1^h \cdot \vec{h}_{1E} \, d\Gamma = 0 \end{aligned} \tag{13}$$

Now we have the correct weak form for our moving mesh. However, this weak form is unstable so we need to use a stabilization scheme to get the stabilized ALE weak form. Here are the stabilization terms to add to the previously found weak form:

$$\sum_{e=1}^{n_{el}} \int_{(\Omega_1)_t} \tau_{SUPS} \left((\vec{u}^h - \hat{\vec{u}}^h) \cdot \nabla \vec{w}_1^h \right) \cdot \vec{r}_M \, d\Omega \sum_{e=1}^{n_{el}} \int_{(\Omega_1)_t} \tau_{SUPS} \left(\frac{\nabla q_1^h}{\rho} \right) \cdot \vec{r}_M \, d\Omega \tag{14}$$

With

$$\tau_{SUPS} = (\frac{4}{\Delta t^2} + \vec{u}^h \cdot \underline{\underline{G}} \vec{u}^h + C_I \nu^2 \underline{\underline{G}} : \underline{\underline{G}})^{-1/2}$$

Where: $\underline{\underline{G}} = \frac{\partial \vec{x}^T}{\partial \vec{x}} \frac{\partial \vec{x}}{\partial \vec{x}}$ is the element metric tensor and C_I is a constant which depends on the element topolgy. This expression of the stabilization term τ_{SUPS} is given by Bazilevs et al (2007). The final expression is as follows:

Stabilized ALE weak form of the Navier-Stokes equations for incompressible flows:

$$\begin{aligned}
&\int_{\Omega_t} \vec{w}^h \cdot \rho \left(\left. \frac{\partial \vec{u}^h}{\partial t} \right|_{\hat{x}} + (\vec{u}^h - \hat{\vec{u}}^h) \cdot \nabla \vec{u}^h - \vec{f}^h \right) d\Omega \\
&+ \int_{\Omega_t} \boldsymbol{\epsilon}(\vec{w}^h) : \underline{\underline{\sigma}} \, d\Omega + \int_{\Omega_t} q^h \nabla \cdot \vec{u}^h \, d\Omega - \int_{\Gamma_E} \vec{w}^h \cdot \vec{h}_E \, d\Gamma = 0 \\
&+ \sum_{e=1}^{n_{el}} \int_{\Omega_t} \tau_{SUPS} \left((\vec{u}^h - \hat{\vec{u}}^h) \cdot \nabla \vec{w}^h \right) \cdot \vec{r}_M \, d\Omega \\
&+ \sum_{e=1}^{n_{el}} \int_{\Omega_t} \tau_{SUPS} \left(\frac{\nabla q^h}{\rho} \right) \cdot \vec{r}_M \, d\Omega = 0
\end{aligned} \tag{15}$$

Later in this report we are going to derive the FEM formulation which will be implemented into the numerical solver.

2.2 Structure mechanics sub-system

Now that we have the final expression for the fluid mechanics sub-system from which we can derive the FEM formulation, we need to obtain the final expression for the structure mechanics sub-system from which we will be able to derive the FEM formulation.

The first step is to derive the equilibrium equation of solids. We consider a body at the time t, we extract from this body an arbitrary surface ΔA and we define the traction vector acting on ΔA as ΔF. The traction vector is as follows:

$$\vec{t} = \lim_{\Delta A \to 0} \frac{\Delta F}{\Delta A} = \underline{\underline{\sigma}} \cdot \vec{n}$$

Where $\underline{\underline{\sigma}}$ is the Cauchy Stress tensor.

Applying this expression to an arbitrary volume $\Delta\Omega$ gives (in a state of equilibrium):

$$\int_{\Delta A} \vec{t} dS = \int_{\Delta A} \underline{\underline{\sigma}} \cdot \vec{n} dS = 0 \tag{16}$$

Since we take an arbitrary volume, this arbitrary volume could be the whole body. Applying the Gauss divergence theorem on the expression for the whole body of (16) we get the strong form of the static equilibrium equation:

$$\boldsymbol{\nabla} \cdot \underline{\underline{\sigma}} = 0$$

Now let's suppose a force field is applied to the body, for example the gravity, we get the forces acting on the body at time t on a volume Ω_t as follows:

$$\int_{\Omega_t} \rho \vec{g} d\Omega$$

Until now, we considered a static equilibrium state, but we can consider a dynamic equilibrium state. In order to do so we just have to add the inertial forces as follows:

$$\int_{\Omega_t} \rho \vec{a} d\Omega$$

Where $\vec{a}$ is the acceleration of the infinitesimal mass corresponding to the volume Ω_t
If we consider any body forces and not specifically the gravity we just replace $\vec{g}$ with $\vec{f}$ and after summing all the terms together, making sure that we put a minus in front of the term for the acceleration because we write the dynamic equilibrium state, and generalizing the expression for any arbitrary ω_t and displacement $\delta\vec{y}$ we get the final expression for the equilibrium:
Cauchy equilibrium equation for solid body:

$$\rho(\vec{a} - \vec{f}) - \boldsymbol{\nabla} \cdot \underline{\underline{\sigma}} = 0 \tag{17}$$

With $\vec{a} = \frac{D\vec{u}}{Dt}$.

Let's derive the weak form of (17). In order to do so, we multiply (17) by the test function $\vec{w}$ which is in the same sort of set defined earlier in the fluid mechanics sub-system. After multiplying we integrate over the domain Ω_t which gives:

$$\int_{\Omega_t} \vec{w} \cdot (\rho(\vec{a} - \vec{f}) - \boldsymbol{\nabla} \cdot \underline{\underline{\sigma}}) d\Omega = 0$$

Now performing an integration by part over the highest derivative term ($-\int_{\Omega_t} \boldsymbol{\nabla} \cdot \underline{\underline{\sigma}} d\Omega$) we get:

$$\int_{\Omega_t} \vec{w} \cdot (\rho(\vec{a} - \vec{f}) d\Omega - \int_{\Gamma_t} \vec{w} \cdot \underline{\underline{\sigma}} \cdot \vec{n} d\Gamma + \int_{\Omega_t} \boldsymbol{\nabla}\vec{w} : \underline{\underline{\sigma}} d\Omega = 0$$

Knowing that $\boldsymbol{\nabla}\vec{w} = \boldsymbol{\nabla}\left(\underline{\underline{\epsilon}} + \underline{\underline{w}}\right)$ with $\underline{\underline{w}}$ being the anti-symmetric part and $\underline{\underline{\sigma}} = \underline{\underline{\underline{\underline{D}}}} : \underline{\underline{\epsilon}}$ is symmetric, we get that

$$\underline{\underline{w}} : \underline{\underline{\underline{\underline{D}}}} : \underline{\underline{\epsilon}} = 0$$

Which means that we finally obtain the following weak form for the solid equilibrium state:

$$\int_{\Omega_t} \vec{w} \cdot (\rho(\vec{a} - \vec{f}) d\Omega - \int_{\Gamma_t} \vec{w} \cdot \underline{\underline{\sigma}} \cdot \vec{n} d\Gamma + \int_{\Omega_t} (\underline{\underline{\epsilon}}(\vec{w}) : \underline{\underline{\underline{\underline{D\epsilon}}}}(\vec{y})) d\Omega = 0$$

$$\Rightarrow \int_{\Omega_t} \vec{w} \cdot (\rho(\vec{a} - \vec{f}) + (\underline{\underline{\epsilon}}(\vec{w}) : \underline{\underline{\underline{\underline{D\epsilon}}}}(\vec{y})) d\Omega - \int_{\Gamma_t} \vec{w} \cdot \underline{\underline{\sigma}} \cdot \vec{n} d\Gamma = 0 \tag{18}$$

Using the definition of the traction vector $\vec{t}$ we get the strong formulation:

$$\int_{\Omega_t} \vec{w} \cdot (\rho(\vec{a} - \vec{f}) + (\underline{\underline{\epsilon}}(\vec{w}) : \underline{\underline{\underline{\underline{D\epsilon}}}}(\vec{y})) d\Omega - \int_{\Gamma_t} \vec{w} \cdot \vec{t} d\Gamma = 0 \tag{19}$$

- $\vec{w} \cdot (\rho(\vec{a} - \vec{f}) + (\underline{\underline{\epsilon}}(\vec{w}) : \underline{\underline{\underline{\underline{D\epsilon}}}}(\vec{y})) = \vec{0}$ for any point $\in \Omega_t$
- $\vec{t} = \vec{0}$ for any point $\in \Gamma_t$
- $\vec{a} = \frac{D\vec{u}}{Dt}, \quad \vec{u} = \frac{D\vec{y}}{Dt}, \quad \vec{y}$ for any point $\in \Gamma_t$

Where $\int_{\Omega_t} \vec{w} \cdot (\rho\vec{a} + \underline{\underline{\epsilon}}(\vec{w}) : \underline{\underline{\underline{\underline{D\epsilon}}}}(\vec{y})) d\Omega$ is the internal virtual work done by the internal stresses within the solid and $-\int_{\Omega_t} \vec{w} \cdot \rho\vec{f} d\Omega - \int_{\Gamma_t} \vec{w} \cdot \vec{t} d\Gamma$ is the external virtual work done by the external forces acting on the boundary and body forces within the domain.
Here we encounter two problems. The first one being that we do not know the configuration of the solid body (domain Ω_t) at the time t, and the second one being that with this expression, we would need to change the domain for the solution of the non-linear problem at each new iteration.
To solve these two problems we will create a reference configuration ($t = 0$) to which every integral and derivation will be done. This will prevent from having to change the domain at each iteration. Every quantity computed will directly be refered to the reference domain.
This is called the Total Lagrangian formulation.
By finding a relationship between the reference density and the current density ($t = 0$), we can find the relationship between the reference and current state of the dynamic equilibrium of the solid. To do so, we will make use of the principle of mass conservation as follows:

$$\frac{dm}{dt} = \frac{d}{dt} \int_{\Omega_t} \rho d\Omega_t = \int_{\Omega_0} \frac{d\rho J}{dt} d\Omega_0 = 0$$

Where $J = \frac{d\Omega_t}{d\Omega_0}$ is the Jacobian which gives a measure of the change in volume between the reference and the current body configuration.

$$\Rightarrow \frac{d\rho J}{dt} = 0$$

$\Rightarrow$ **Equation of conservation of mass:** $\rho J = \rho_0 J_0 = \rho_0$ Let's introduce the deformation gradient that is subsquent to the displacement from reference to current body configurations:

$$\underline{\underline{F}} = \boldsymbol{\nabla}_X \vec{x}$$

With this deformation gradient we can introduce the first Piola-Kirchhoff stress tensor:

$$\underline{\underline{P}} = J\underline{\underline{\sigma F}}^{-T}$$

To get the Total Lagrangian formulation in reference configuration we need to apply a transformation of coordinates to the traction term $\vec{t}$:

$$\underline{\underline{F}}^T \vec{\hat{t}} d\Gamma \Big|_X = \vec{t} d\Gamma \Big|_x$$

Plugging the equation of conservation of mass, the expression of the deformation gradient and the first Piola-Kirchhoff stress tensor inside (19) gives the strong formulation:

$$\int_{\Omega_0} \vec{w} \cdot (\rho_0(\vec{a} - \vec{f}) - \boldsymbol{\nabla}_X \cdot \underline{\underline{P}} d\Omega + \int_{\Gamma_0} \vec{w} \cdot \underline{\underline{P}} \cdot \vec{\hat{t}} d\Gamma = 0 \tag{20}$$

- $\rho_0(\vec{a} - \vec{f}) - \boldsymbol{\nabla}_X \cdot \underline{\underline{P}} = \vec{0}$ for any point $\in \Omega_0$
- $\underline{\underline{P}} \cdot \vec{\hat{t}} = \vec{0}$ for any point $\in \Gamma_0$
- $\vec{a} = \frac{D\vec{u}}{Dt}, \quad \vec{u} = \frac{D\vec{g}}{Dt}, \quad \vec{y} = \vec{g}$ for any point $\in \Gamma_0$

Now, what is left to do (as in the fluid dynamics sub-system) is to use FEM methods to solve $\underline{\underline{KU}} = \underline{F}$ for $\underline{U}$.

2.3 Mesh-motion sub-system

In a Fluid Structure Interaction problem there is two domains, the fluid domain and the structure domain. These two domains interact together with forces, magnetic fields etc... When using FEM to represent the two domains, there is two possibilities. We can use a non-moving grid method or a moving-grid method. The first one allows the solid's finite element grid to overlap the fluid's. By overlapping, the fluid grid doesn't move and the volume boundary conditions are applied to the previously occupied volume by the solid. This method can be useful for problems with big structural motions like changes in the topology. However, our problem doesn't change in topology nor have big structural motions which means that we will prefer using a moving grid method.
This method is called the Solid Extension Mesh Motion Technique (SEMMT). With this method, the two sub-systems previously derived (fluid and structure mechanics) are coupled at the interface allowing for real physically meaningful interface conditions. SEMMT is a Lagrangian description of the solid's motion, which is in accordance to the Total Lagrangian formulation we just derived. However, the fluid mechanics domain must be incorporated into the differential equations and boundary conditions as a consequence of the moving interface. because SEMMT is a moving-mesh method, it is very efficient in terms of computational costs as it doesn't need to remesh at every iteration.
Let's now derive the mathematical model of the SEMMT method.
The fluid domain mesh can be treated as a linear elastic solid. This allows us to formulate the variational formulation of linear elasticity for a 3D solid as follows:
Find $\vec{\tilde{y}} \in S_m$ such that $\forall \vec{w} \in V_m$:

$$\int_{\Omega_{\tilde{t}}} \underline{\underline{\epsilon}}(\vec{w}) \cdot \underline{\underline{\underline{\underline{D\epsilon}}}}(\vec{\tilde{y}} - \vec{\tilde{y}}(\tilde{t})) = 0$$

Where:

- $\Omega_{\tilde{t}}$ is the domain at the previous timestep
- $\vec{\tilde{y}}(\tilde{t})$ is the know displacement of the fluid domain at previous timestep
- $\tilde{t}$ is the previous timestep

- $\underline{\underline{\epsilon}}$ is the linear strain

Since we are using the ALE method for the fluid mechanics sub-system, we need the velocity of the flui domain which can be computed as follows:

$$\vec{\hat{u}} = \left.\frac{d\vec{\hat{y}}}{dt}\right|_{\hat{x}}$$

Non-overlapping is one the most critical part of SEMMT. In order to prevent this from happening, we need to impose strong and coherent boundary conditions such as:

$$\begin{cases} \vec{\hat{y}} \cdot \vec{n} = \vec{y} \cdot \vec{n} \quad on \quad \Gamma_t \\ \\ \vec{w} \cdot \vec{n} = 0 \quad on \quad \Gamma_t \end{cases} \tag{21}$$

We will see later in the report that we have matching meshes, susbequent to this these two boundary conditions become:

$$\begin{cases} \vec{\hat{y}} = \vec{y} \quad on \quad \Gamma_t \\ \\ \vec{w} = 0 \quad on \quad \Gamma_t \end{cases} \tag{22}$$

In order to correctly model the motion of the fluid domain mesh we need to define the proper elastic tensor $\underline{\underline{\underline{\underline{D}}}}$. A good elastic tensor should allow to:

- Control the quality of the mesh during the motion by allocating correct element size and regularity with respect to gradients in the mesh
- Preserve the boundary structure of the mesh as designed in the fixed initial reference

To do so we link the Lamé coefficients to the cell volume or shape in order to correlate the prerequisites above with fluid domain stiffness. Meaning the smaller the cell the stiffer:

$$\begin{cases} \mu^h = \frac{E_m^h}{2(1+\nu_m)} \\ \\ \lambda^h = \frac{\nu_m E_m^h}{(1+\nu_m)(1-2\nu_m)} \end{cases} \tag{23}$$

Finally, we can obtain the FEM formulation for the solver to solve $\underline{\underline{KY}} = \underline{F}$ for $\underline{Y}$.

2.4 Interface conditions for FSI

In a an FSI problem, no matter what kind of mesh-moving technique one's using, one of the most crucial part of the definitions of the problem is interface conditions. Indeed, it is at the interface between the solid and the fluid domain that all 3 sub-systems interact with one another meaning that the definition of the meshes and the conditions at the interface between the solid and the fluid is at utmost importance. Interfaces in FSI problems exchange a lot of information and need to be well defined in order for the problem to be correctly solved and with consistency. The first step is to choose how to set up the interface in terms of meshes. Meaning, choosing between a matching and non-matching grid mesh interface (see Figure 2). The non matching grid mesh

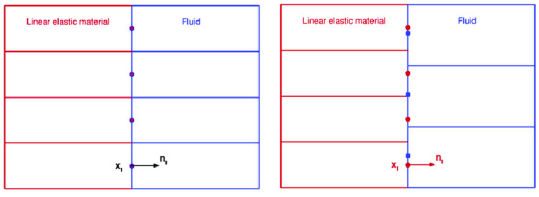

Figure 2: Simple schematic of a matching (left) and non matching (right) grid mesh interface

is very convenient for complex interfaces between the fluid and the structure domain as it allows for different mesh refinements in the same area to allow better accuracy of the solution for example. However, because the grids of the different meshes do not match (the points of the fluid domain's mesh are not the same as the solid domain's), the operator has to make sure that the kinematics and tractions have the same coupling. In order to do so, he must interpolate/project the solution and quantities computed at each point of one interface surface (for example the fluid domain interface) to the points of the other interface surface which requires more

mathematical complexity.
The matching grid mesh interface is much less complex in terms of mathematical models and FSI coupling conditions. This case is very efficient for simple fluid-structure geometries where we do not need to refine in specific areas to obtain satisfactory results and good consistency. However, the downside is much less flexibility in discretization choices which means that one must make sure that his discretization is well defined and all interfaces are correctly matching. The less flexibility one has, the less complex the FSI problems.
Conveniently, our FSI problem do not have complex fluid-strtucture interfaces which means we do not require the complex non matching grid mesh technique.

Let's now derive the boundary conditions and compatibility equations that will be applied to the fluid and structure domains.
For the following mathematical equations, all subscripts $_1$ will refer to the fluid domain, all subscript $_2$ will refer to the solid domain and all subscripts $_3$ will refer to the mesh domain.
First, let's remark that the structure's surfaces have a velocity due to the deformation caused by the fluid. In order for the fluid and solid domain's interfaces to act like one (meaning the surface of the solid domain is the exact same as the fluid domain's) and won't overlap each other we have to impose kinematic compatibility:

$$\vec{u} = \frac{d\vec{y}}{dt} \quad on \quad \Gamma_1$$

We also need to compute the mesh velocity at every point of the fluid domain to use it inside the ALE method:

$$\vec{\hat{u}} = \left.\frac{d\vec{\hat{y}}}{dt}\right|_{\hat{x}} \quad on \quad \Gamma_1$$

We can summurize these interface interactions in a simple schematic:

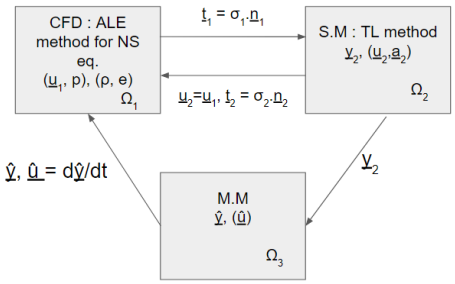

Figure 3: Simple schematic of the interactions between the fluid domain (Ω_1), the structure domain (Ω_2) and the mesh domain (Ω_3)

2.5 FSI coupling

As seen before, FSI problems require coupling between solutions acquired from 3 different domains. Indeed, in order to get the numerical results of the interaction of a fluid on a structure, the solver needs to couple the solutions computed for the fluid mechanics sub-system, the solution computed for the structure mechanics sub-system and the one computed for the moving mesh sub-system.
Now that we have the 3 variational equations for our ALE-FSI problem:

Find, $u^h \in S_u^h, p^h \in S_p^h, y^h \in S_y$, such that $\forall \vec{w}_1^h \in V_u^h, q^h \in V_p^h, \forall \vec{w}_2^h \in V_y^h$

$$
\begin{cases}
\textbf{Stabilized ALE:} \\
\int_{\Omega_t} \vec{w}^h \cdot \rho \left(\left. \frac{\partial \vec{u}^h}{\partial t} \right|_{\hat{x}} + (\vec{u}^h - \hat{\vec{u}}^h) \cdot \nabla \vec{u}^h - \vec{f}^h \right) d\Omega \\
+ \int_{\Omega_t} \boldsymbol{\epsilon}(\vec{w}^h) : \underline{\underline{\sigma}}\, d\Omega + \int_{\Omega_t} q^h \nabla \cdot \vec{u}^h \, d\Omega - \int_{\Gamma_E} \vec{w}^h \cdot \vec{h}_E \, d\Gamma = 0 \\
+ \sum_{e=1}^{n_{el}} \int_{\Omega_t} \tau_{SUPS} \left((\vec{u}^h - \hat{\vec{u}}^h) \cdot \nabla \vec{w}^h \right) \cdot \vec{r}_M \, d\Omega \\
+ \sum_{e=1}^{n_{el}} \int_{\Omega_t} \tau_{SUPS} \left(\frac{\nabla q^h}{\rho} \right) \cdot \vec{r}_M \, d\Omega = 0 \\
\\
\textbf{TL formulation of non linear structure dynamics:} \\
\int_{(\Omega_2)_t} \vec{w}_2^h \cdot \rho_2 \left(\frac{d\vec{y}^h}{dt} - \vec{f}_2^h \right) d\Omega + \int_{(\Omega_2)_t} \underline{\underline{\epsilon}}(\vec{w}_2^h) : \underline{\underline{\underline{\underline{\sigma_2}}}}\, d\Omega - \int_{\Gamma_{1E}} \vec{w}_2^h \cdot \vec{h}_{2E}^h \, d\Gamma \\
\\
\textbf{SEMMT:} \\
\int_{(\Omega_1)_t} \underline{\underline{\epsilon}}(\vec{w}_3^h) \cdot \underline{\underline{\underline{\underline{D\epsilon}}}} \left(\vec{\hat{y}}^h - \vec{\hat{y}}^h(\tilde{t}) \right) d\Omega = 0
\end{cases}
\tag{24}
$$

Now let's derive their respective FEM formulations.
Notation: $_A$ is the global node of the element on which the computations occur, $N_A(\vec{x})$ is the shape function of the element on the global node A.
The FEM approximations of the test functions from the variational equations above are:

- $(w_1^h)_i = \sum_A (w_1)_{A,i} N_A(x)$
- $q_1^h = \sum_A (q_1)_A N_A(x)$
- $(w_2^h)_i = \sum_A (w_2)_{1,i} N_A(x)$
- $(w_3^h)_i = \sum_A (w_3)_{A,i} N_A(x)$

Substituting these FEM approximations in the variational equations of the system (24) we get:

$$\sum_A (w_1)_{A,i}[(N_{1M})_{A,i}] + \sum_A (q_1)_A[(N_{1C})_A] + \sum_A (w_2)_{1,i}[(N_2)_{A,i}] + \sum_A (w_3)_{A,i}[(N_3)_{A,i}] = 0$$

where we can seperate the different vectors containing the contributions from the different sub-systems to the final solution:

- $\vec{N}_{1M} = [(N_{1M})_{A,i}]$ is the ALE NS momentum
- $\vec{N}_{1M} = [(N_{1C})_A]$ is the ALE NS continuity
- $\vec{N}_2 = [(N_2)_{A,i}]$ is the structure dynamics
- $\vec{N}_3 = [(N_3)_{A,i}]$ is the moving mesh

Now recall that the discretized trial functions are $\vec{u}^h, p^h$ for the fluid domain, $\vec{y}^h = \vec{g}^h$ for the structure domain and $\vec{\hat{y}}$ for the moving mesh. We can define the FEM approximations of the trial functions on global node B like previously done for the test functions. Now let's define the vectors which contain the solutions at the nodes and their derivatives with respect to the time:

- $\vec{P} = \{p_B\}; \quad \vec{U} = \{u_{B,i}\}; \quad \dot{\vec{U}} = \{\dot{u}_{B,i}\}$
- $\vec{Y} = \{u_{B,i}\}; \quad \dot{\vec{Y}} = \{\dot{y}_{B,i}\}; \quad \ddot{\vec{Y}} = \{\ddot{y}_{B,i}\}$
- $\vec{\hat{Y}} = \{\hat{y}_{B,i}\}; \quad \frac{\partial \vec{\hat{Y}}}{\partial t} = \{\frac{\partial \hat{y}}{\partial t}\}; \quad \frac{\partial^2 \vec{\hat{Y}}}{\partial^2 t} = \{\frac{\partial^2 \hat{y}}{\partial^2 t}\}$

We finally get the general FEM system of equations:

$$\begin{cases} \vec{N}_{1M}(\vec{\dot{U}}, \vec{U}, \vec{P}, \vec{\ddot{Y}}, \vec{\dot{Y}}, \vec{Y}, \frac{\partial^2 \vec{Y}}{\partial^2 t}, \frac{\partial \vec{Y}}{\partial t}, \vec{\hat{Y}}) = 0 \\ \vec{N}_{1C}(\vec{\dot{U}}, \vec{U}, \vec{P}, \vec{\ddot{Y}}, \vec{\dot{Y}}, \vec{Y}, \frac{\partial^2 \vec{Y}}{\partial^2 t}, \frac{\partial \vec{Y}}{\partial t}, \vec{\hat{Y}}) = 0 \\ \vec{N}_{2}(\vec{\dot{U}}, \vec{U}, \vec{P}, \vec{\ddot{Y}}, \vec{\dot{Y}}, \vec{Y}, \frac{\partial^2 \vec{Y}}{\partial^2 t}, \frac{\partial \vec{Y}}{\partial t}, \vec{\hat{Y}}) = 0 \\ \vec{N}_{3}(\vec{\dot{U}}, \vec{U}, \vec{P}, \vec{\ddot{Y}}, \vec{\dot{Y}}, \vec{Y}, \frac{\partial^2 \vec{Y}}{\partial^2 t}, \frac{\partial \vec{Y}}{\partial t}, \vec{\hat{Y}}) = 0 \end{cases} \tag{25}$$

This system of equations, however, is non-linear and time-dependent. We will need 3 iterative methods to solve the system:

- A numerical time integration method : we choose the Generalized-α scheme
- An iterative method: we choose Newton-Raphson method
- A sparse linear solver: we choose GMRES

The Generalized-α scheme is a time integration method using different parameters to tune the accuracy of the integration. The main point of this method is to calculate the solutions at the next timestep using the solution computed at an intermediate timestep. This intermediate timestep is the $t + \alpha$ time step. When using this scheme, we can tune 2 parameters which define it:

- α_m which is the numerical damping associated with the mass matrix of equation of motion of the problem
- α_f which is the numerical damping associated with the force vector

With: $\frac{1}{2} \leq \alpha_f \leq \alpha_m$ When applying the Generalized-α scheme as part of the multicorrector phase and substituting the expressions of the scheme into the semi-discrete system (25) we find that some variables are dependent to others. Meaning we can simplify and rewrite (25):

$$\begin{cases} \vec{N}_{1M}(\vec{\dot{U}}_{n+1}, \vec{P}_{n+1}, \vec{\ddot{Y}}_{n+1}, \vec{\hat{Y}}_{n+1}) = 0 \\ \vec{N}_{1C}(\vec{\dot{U}}_{n+1}, \vec{P}_{n+1}, \vec{\ddot{Y}}_{n+1}, \vec{\hat{Y}}_{n+1}) = 0 \\ \vec{N}_{2}(\vec{\dot{U}}_{n+1}, \vec{P}_{n+1}, \vec{\ddot{Y}}_{n+1}, \vec{\hat{Y}}_{n+1}) = 0 \\ \vec{N}_{3}(\vec{\dot{U}}_{n+1}, \vec{P}_{n+1}, \vec{\ddot{Y}}_{n+1}, \vec{\hat{Y}}_{n+1}) = 0 \end{cases} \tag{26}$$

With the subscript $_{n+1}$ being the time iteration subscript.

Let's introduce the coupling algorithm we are going to use for this project work. We chose a strongly-coupled algorithm, as opposed to loosely-coupled. Strongly-coupled algorithms solve the fluid, structure and mesh equations simultaneously and use immediately in the same block the solutions of each domain for each other domain. They have two main advantages being an increased robustness in comparison to the loosely-coupled counterpart and an increased stability associated with a better convergence. The big downside of such algorithm is the set up which means writing an entire FSI solver which takes time and effort. The particular algorithm we will use is the Block Iterative solver.
Let's introduce a generalized form of the semi-discrete system derived previously:

$$\begin{cases} \vec{N}_1(\vec{d}_1, \vec{d}_2, \vec{d}_3) = 0 \\ \vec{N}_2(\vec{d}_1, \vec{d}_2, \vec{d}_3) = 0 \\ \vec{N}_3(\vec{d}_1, \vec{d}_2, \vec{d}_3) = 0 \end{cases} \tag{27}$$

With $\vec{N}_1$ containing both continuity and momentum contributions.

- $\vec{d}_1$ contains the fluid dynamics unknowns

- $\vec{d}_2$ contains the structure dynamics unknowns
- $\vec{d}_1$ contains the mesh dynamics unknowns

The Newton-Raphson method allows to solve the following subsequent linear system of equations:

$$\begin{aligned}
\underline{\underline{\underline{A}}}_{11}\,\Delta\vec{d}_1 + \underline{\underline{\underline{A}}}_{12}\,\Delta\vec{d}_2 + \underline{\underline{\underline{A}}}_{13}\,\Delta\vec{d}_3 &= -\vec{N}_1 \qquad & \vec{d}_1^{\,i+1} &= \vec{d}_1^{\,i} + \Delta\vec{d}_1 \\
\underline{\underline{\underline{A}}}_{21}\,\Delta\vec{d}_1 + \underline{\underline{\underline{A}}}_{22}\,\Delta\vec{d}_2 + \underline{\underline{\underline{A}}}_{23}\,\Delta\vec{d}_3 &= -\vec{N}_2 \qquad & \vec{d}_2^{\,i+1} &= \vec{d}_2^{\,i} + \Delta\vec{d}_2 \\
\underline{\underline{\underline{A}}}_{31}\,\Delta\vec{d}_1 + \underline{\underline{\underline{A}}}_{32}\,\Delta\vec{d}_2 + \underline{\underline{\underline{A}}}_{33}\,\Delta\vec{d}_3 &= -\vec{N}_3 \qquad & \vec{d}_3^{\,i+1} &= \vec{d}_3^{\,i} + \Delta\vec{d}_3
\end{aligned}$$

With $\underline{\underline{\underline{A}}}_{xy} = \frac{\partial \vec{N}_x}{\partial \vec{d}_y}$.

Each equation is solved isolating the wanted linear equation (for example: $\underline{\underline{\underline{A}}}_{11}\,\Delta\vec{d}_1 = -\vec{N}_1 + ...$) by putting the correct terms to the right-hand side of the equation and solving by inverting the matrix (in the same example, inverting $\underline{\underline{\underline{A}}}_{11}$) using the chosen linear solver (in our case GMRES). The values for the terms in the RHS of the equation are taken from the most current values previously computed. Then we update the vector containing the solutions of the domain for which we just computed the solutions and we use this updated vector to compute the solutions of the next domain.
Here is a schematic of the block iterative algorithm taken from the lecture slides 11 of the course Fluid Structure Interactionof Professor Alessio Castorrini:

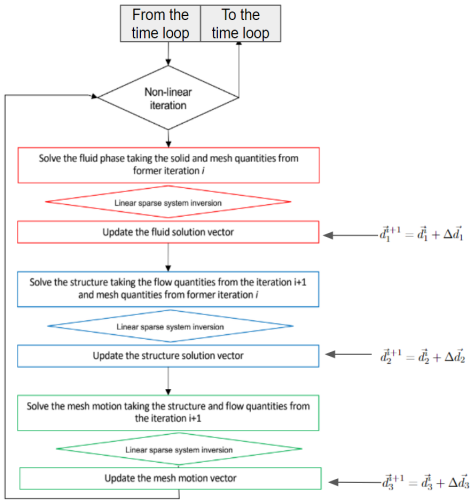

Figure 4: Simple schematic of the Block iterative algorithm

Now that we have discretized the theoretical equations of each sub-system and implemented them into wisely chosen numerical algorithm schemes and methods in order to create an FSI solver for our problem, we can jump into the numerical setup of the fluid flow in a pipe-like problem.

3 Numerical setup

3.1 Mesh

The first step in the numerical setup is to create the mesh. As we saw, in an FSI problem we have two meshes, one for the fluid domain and one for the structure. Because we are using a matching grid mesh interface, it is very important to set the same number of nodes at the surfaces of the interfaces between the fluid and structure meshes like in the Figure 5.

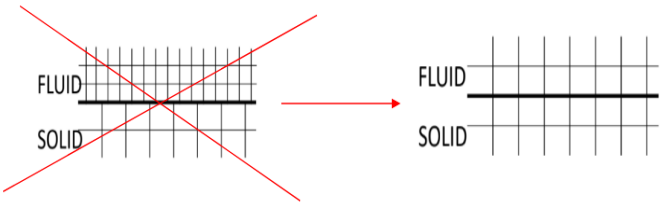

Figure 5: Schematics of the correct grid we want to have

The density of the mesh is very important as well because the denser the mesh, the more accurate the results are. Meaning that we want a correct amount of elements in both meshes that will be able to give satsifying results with good accuracy without asking for too much computation power. However, density is not the only characteristic to take into account. Indeed, we need a smooth mesh accross the whole geometry because rough changes in number of elements in meshes cause instabilities (as I experienced with the first mesh I created) which means we need to be careful on how we set up the number of points on each geometrical element of the domains. See Figure 6 for the actual fluid and structure meshes used for the project work.

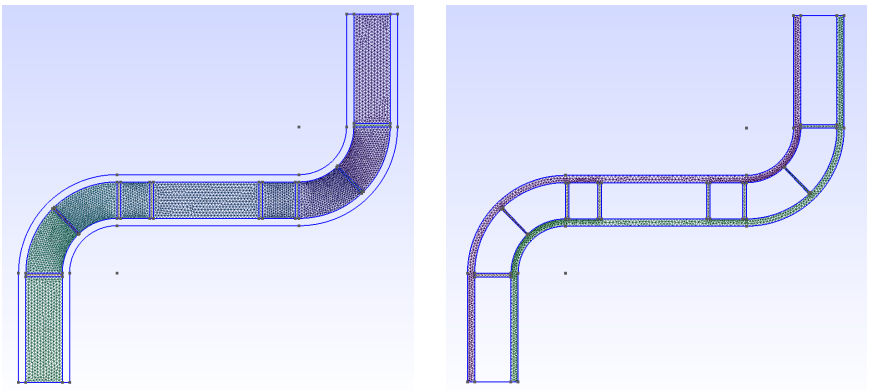

Figure 6: Fluid domain's mesh (left) and structure domain's mesh (right)

- Fluid mesh number of nodes: 4416
- Fluid mesh number of elements: 9550
- Structure mesh number of nodes: 2415
- Structure mesh number of elements: 4948

3.2 Boundary conditions

In order to have a problem well posed and as close to reality as possible, we need to add the correct boundary conditions. For this fluid flow in a pipe-like problem we have 4 Dirichlet boundary conditions:

- $(\vec{u}_1)_y\Big|_{inlet}$ = value set by the user
- $(\vec{u}_1)_x\Big|_{inlet} = 0$
- $\vec{y}_2\Big|_{inlet} = \vec{y}_2\Big|_{outlet} = 0$

Because the velocity of the fluid at the outlet is unknown, we don't set any boundary condition for the fluid domain at the outlet. As we want to study the displacements (and the stresses) of a pipe-like structure subject to internal flow of a fluid, we don't set any boundary condition for the structure domain at the fluid-structure interface as well as on the exterior of the pipe so that it can move freeely.

4 Case studies

Before runing the simulations, we need to "apply" initial conditions for the solver to solve the discretized problem using stabilized previous solutions. This will allow for the solver to give consistent results. In order to do so, we run an "initial simulation" for 20 timesteps that would last 2 seconds in real life ($dt = 0.1$) with parameters that we know for sure will produce stable solutions with a relatively high dt. Here we ran the initial simulations with a Young's modulus for the pipe-like structure of the order of 10^{12} and a low Reynold's number. This Young's modulus is very high, thus preventing the structure from deforming excessively and allowing for the fluid flow to flow laminarly through the entire pipe-like structure. The simulations that will be presented in the next part are simulations that start from the 20th timestep, thus allowing for the solver to start with the stabilized solutions through the entire domain of the previous timestep of the initial simulation.

4.1 Arbitrary case study with real-world parameters

In this case study we chose to run the simulation for water flowing inside a pipe-like structure with a Young's modulus of 0.1 GPa which is, according to **BesTech sensors and equipment**[2], the modulus of strong rubber. We wanted to model some sort of malfunction of the pump system which makes the fluid flow through the rubber pipe. We imposed a constant flow velocity of 1.5 m/s which is, according to **Corzan material & piping solutions**[3], the typical flow velocity inside a pipe, with a sudden burst in velocity at 5.4 m/s representing the malfunction of the pump system (see Figure 7). The timestep dt is set to 0.005, a satisfying timestep that we found after runing multiple simulations with different timesteps.

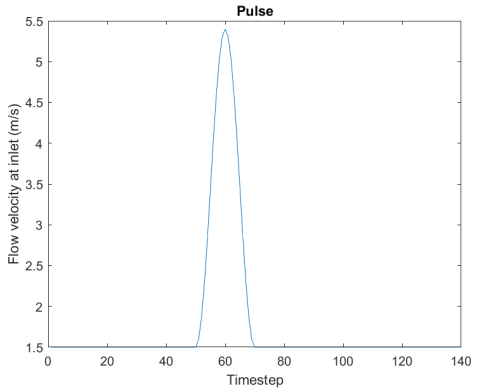

Figure 7: Flow velocity as a function of the time iteration

4.2 Results

[Click here] to watch the video of water flowing inside a rubber pipe with displacement and velocity scales (in meters and m/s respectively

[Click here] to watch the video of water flowing inside a rubber pipe with stresses (σ) and velocity scales (in Pascals and m/s respectively)
Here are screenshots from Paraview of notable frames of the simulation of water flowing inside a rubber pipe:

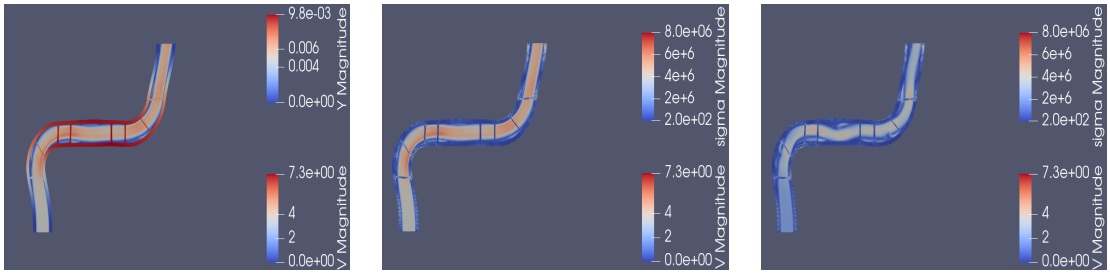

Figure 8: (From left to right) Frame for which the displacement is the highest, same frame but displaying the stresses (σ), frame displaying some vortices shading

Analysing these results we see that the maximum displacement is 9.3 mm, the maximum velocity is 7.3 m/s and the maximum stress is 8 MPa. We can easily understand that a stong rubber pipe would not have huge amounts of displacement when subjected to a water flow from its inside. Which is why the maximum displacement given by the scale of Paraview is acceptable and can be taken into account. Having said that, we can say that, 9.3 mm represents around $\frac{1}{10}^{th}$ of the longitudinal length of the pipe which would need further analysis and engineering thinking to conclude on whether it is acceptable or not for the specific application. As for the stresses, we see that the maximum stresses according to the scale of Paraview (which has been set to compute the scale using all timesteps) is 8 MPa but in the video we observe that the structure never reaches a red coloring. At most it reaches a white coloring which would be $\sim$4 MPa. Anyway, according to **Chevalier cléret**[4] rubbers break for stresses between 10 to 30 MPa and according to **MatWeb**[5] the average ultimate tensile stress of rubbers is 7 MPa, with the ultimate tensile strength ranging from 0.138 to 165 MPa depending on the type of rubber. Taking everything into account, we can say that the strong rubber pipe did not break. What could also be interesting to notice is the formation of vortices when the burst of velocity occurs. This could lead to perturbations further inside the pipe. We also observe a maximum velocity of 7.3 m/s which is more than the velocity of the burst. For engineering purposes and applications, this delta of velocity between the velocity of the burst and the actual maximum velocity reached by the water flow inside the rubber pipe is important to notice and take into account.

4.3 Real-world case study

Now that we have analysed a simulation of a pipe-like structure with parameters taken from real-world values but adding an arbitrary change (the burst), it is time to make a simulation of a real-world application. We will be simulating the blood flow through a typical vein of the body. We will go a little bit further than that by imagining that we are simulating the blood flow induced by the heart helped by a pacemaker which will have a malfunction. This malfuncion, although almost impossible with current pacemaker since they are highly efficient and safe, will act like if it sent a wrong signal to the heart which made the heart to pump too much for one pump. For the properties of the pipe-like structure modeling a vein we chose an inner diameter of 5000 μm and a wall thickness of 500 μm [6], a Young's modulus of 4.2 MPa [7] and a density of 1060 g/cm^3 [8]. As for the blood flow, we make a strong but acceptable assumption of a Newtonian fluid which is the academically accepted assumption for numerical simulations of blood flow. As for the properties of the fluid, in order to be accurately modeling blood, we chose to set the density at 1050 km/m^3 [9]. For the kinematic viscosity, according to the National Center for Biotechnology Information[10], blood kinematic viscosity ranges from 3.5×10^{-6} to 5.5×10^{-6} $Pa.s$ where as in the article Magnetic Field Effects on 3D Blood Flow Patterns of Straight and Stenotic Arteries[9] where they make numerical simulations of blood flow they chose a kinematic viscosity for blood of 3.1e-6 $Pa.s$. Because the value from [9] and the range given by [10] are very similar we will be using the value from the article [9] since we are also numerically modeling blood in this project work. As for the blood flow velocity, we will be simulating the pumping motion of blood flow by the heart using a sinusoidal equation. In our simulation, in its normal regime, the heart pumps blood at 0.045 m/s [11]. However, when the malfunction occurs, we imagine an important malfunction which leads to the blood flow velocity being higher than the maximum blood flow velocity of 0.071 m/s [11] (see Figure 9). We will be setting the malfunctioning blood flow velocity to 0.075 m/s.
The geometrical changes to the pipe-like structure induce slight changes to the number of elements and nodes of the fluid and structure meshes:

- Fluid mesh number of nodes: 4418
- Fluid mesh number of elements: 9554
- Structure mesh number of nodes: 1799
- Structure mesh number of elements: 3716

These changes are little and as we found out later on when runing simulations, don't induce problems.

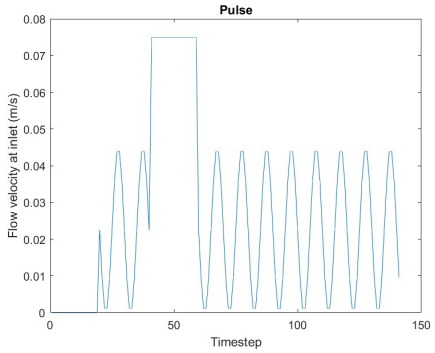

Figure 9: Flow velocity as a function of the time iteration

4.4 Results

[Click here] to watch the video of blood flowing inside a vein with displacement and velocity scales (in meters and m/s respectively

[Click here] to watch the video of blood flowing inside a vein with stresses (σ) and velocity scales (in Pascals and m/s respectively)
Here are screenshots from Paraview of notable frames of the simulation of blood flowing inside a vein:

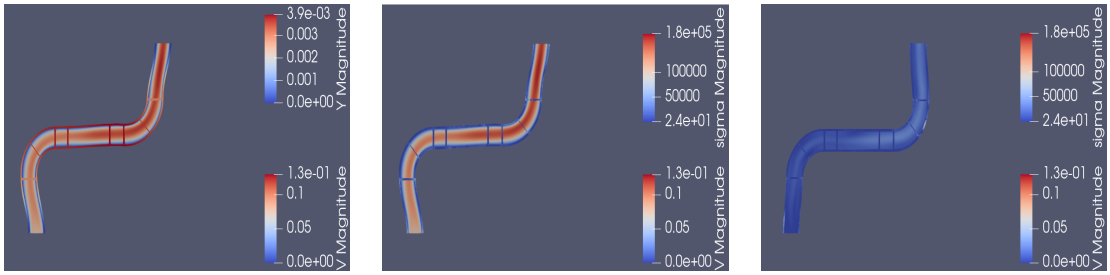

Figure 10: (From left to right) Frame for which the displacement is the highest, same frame but displaying the stresses (σ), frame displaying some a small point of high stresses

Analysing these results, we see that the highest displacement of the structure is 3.9 mm which is of the order of the diameter of the vein (or less than $\frac{1}{10}^{th}$ of the longitudinal length of the vein), the maximum velocity is 0.13 m/s and the maximum stresses are 0.18 MPa. When analysing the picture on the right of Figure 10 we can see a spot of high stresses on the 2^{nd} right-angled turn. The frame from which this screenshot has been taken is few frames after the end of the burst of flow velocity from the malfunction. This could mean that the burst of blood flow velocity might causes damages to the vein. However, the stresses at this point on this frame are ~ 0.1 MPa which is low. Sapheneous veins, which are the kind of vein we took parameter for the simulation from, have an ultimate tensile strength taht ranges from 1.5 MPa to 4 MPa [12]. The article [13] states that the ultimate circumferential tensile strength of sapheneous veins with the same Young's modulus that we set for our vein is 1.8 MPa. If we take into account the maximum stresses indicated by the scale of Paraview, we can conclude that the vein would break. However, when looking at the video of the simulation, we notice that the stresses on the vein that reach this value are on the last frame and near the outlet which would not seem true to reality. We can assume these stresses as an error by the solver and choose to not take them into account. That would mean that the stresses of the picture on the right of Figure 10 would be the biggest ones occuring in the vein walls. These stresses being 0.1 MPa, we can conclude that the vein doesn't break. What can be interesting to notice as well is the maximm displacement. Indeed, it is of order of the diameter of the vein which is not a lot when comparing it to the maximum velocity the blood flow reaches. This maximum velocity is 0.13 m/s which is a lot more than the maximum velocity blood flow can reach according to [11]. This means that in such abnormal case of malfunction, the vein would only move of the order of its inner diameter. Of course this is not taking into account the eventual forces applied on the exterior of the vein by the surrounding tissues. Finally, the maximum velocity follows the same kind of scheme as for the simulation of a burst of water flowing inside a rubber pipe where it is higher than the velocity of the burst.

5 Conclusion and discussion

In both simulations, significant insights were gained into the behavior of the rubber pipe and the saphenous vein under burst flow conditions.

For the rubber pipe, the maximum displacement observed was 9.3 mm, which is approximately one-tenth of its longitudinal length. While this displacement is substantial, it is within acceptable limits for a strong rubber pipe subjected to internal water flow. The maximum stress recorded was 8 MPa, which is below the breaking threshold for rubber materials, which ranges between 10 to 30 MPa according to Chevalier Cléret [4] and MatWeb [5]. Additionally, the presence of vortices indicates potential perturbations inside the pipe, which could impact its structural integrity. The observed maximum velocity of 7.3 m/s exceeded the initial burst velocity, highlighting a critical aspect for engineering applications.
In the case of the saphenous vein, the highest displacement was 3.9 mm, which is less than one-tenth of its longitudinal length and of the order of its diameter. The maximum velocity recorded was 0.13 m/s, significantly higher than typical blood flow velocities. The maximum stress observed was 0.18 MPa, with a localized peak of 0.1 MPa at a critical turn in the vein, suggesting potential vulnerability at this point. However, these stresses are well below the ultimate tensile strength of saphenous veins, which ranges from 1.5 to 4 MPa, indicating that the vein would not break under the simulated conditions.

Both scenarios emphasize the importance of considering maximum displacements, stresses, and velocities in assessing the structural integrity of materials under burst flow conditions. The rubber pipe and the saphenous vein, despite different material properties and applications, exhibit similar stress and displacement behaviors that inform their respective tolerances and potential vulnerabilities. Further detailed analysis and engineering judgment are necessary to fully evaluate the implications of these findings for practical applications.
Given more time, studying the frequency of vibration of the pipe-like structure which we can start to see after the burst of velocity in the video of the rubber pipe would be interesting. Indeed, The frequency response of a mechanical system subjected to external forces is a crucial point for assessing the viability of the system for the specific engineering application. If the pipe-like structure is resonating at its natural frequencies, it will most definitely break at a certain time.

While the results obtained from the simulations are insightful, there are several avenues for further analysis and improvement to achieve more accurate and comprehensive results:

- **Material Properties**: The accuracy of the simulations heavily depends on the material properties used. For more precise results, it would be beneficial to conduct experimental tests to obtain detailed material properties for both the rubber pipe and the saphenous vein. This includes non-linear stress-strain behavior, viscoelastic properties, and fatigue characteristics.
- **Mesh Refinement and Adaptivity**: The quality of the computational mesh can significantly affect the simulation results. Employing finer meshes and adaptive mesh refinement techniques can help capture localized phenomena more accurately, such as stress concentrations and vortex formations. However, this will increase the computational cost and require efficient algorithms to manage the trade-off between accuracy and computational feasibility.
- **Fluid-Structure Interaction Models**: Enhancing the fidelity of the fluid-structure interaction (FSI) models can lead to better predictions. Incorporating more advanced turbulence models, could provide a more detailed understanding of the flow dynamics and their interaction with the structural components.
- **Boundary Conditions**: The boundary conditions applied in the simulations are critical for realistic results. More accurate representations of the physical environment, including external loads, constraints, and interactions with surrounding tissues (in the case of the vein), can lead to more realistic simulations. In the case of biomedical applications, patient-specific data can be used to tailor the simulations to individual scenarios.
- **Parametric Studies and Sensitivity Analysis**: Conducting parametric studies to understand the sensitivity of the results to various input parameters can provide deeper insights into the critical factors influencing the system's behavior. This can help identify the most significant parameters and guide future experimental and simulation efforts.
- **Coupled Multi-Physics Simulations**: Integrating additional physical phenomena into the simulations, such as thermal effects, chemical reactions (e.g., in biomedical applications), or electrical fields, could provide a more holistic view of the system's response under various conditions.

References

[1] A. Castorrini and F. Rispoli, "Fluid structure interaction," 2024.

[2] *Bestech sensors and equipment.* [Online]. Available: https://www.bestech.com.au/wp-content/uploads/Modulus-of-Elasticity.pdf.

[3] *Corzan material piping solutions: How to design an industrial piping system for ideal flow rate and velocity.* [Online]. Available: https://www.corzan.com/en-us/blog/how-to-design-an-industrial-piping-system-for-ideal-flow-rate-and-velocity.

[4] *Chevalier cléret: Rubber tensile strength and elongation at break.* [Online]. Available: https://www.chevalier-cleret.de/technische-ereignisse/rubber-tensile-strength-and-elongation-at-break.html#:~:text=Depending%20on%20mixtures%20and%20on,between%204%20and%2010%20MPa.

[5] MatWeb. "Matweb: Overview of materials for silicone rubber." (), [Online]. Available: https://www.matweb.com/search/datasheet.aspx?matguid=cbe7a469897a47eda563816c86a73520.

[6] B. Müller, S. Lang, M. Dominietto, *et al.*, "High-resolution tomographic imaging of microvessels," *Proc SPIE*, vol. 7078, 70780B, Aug. 2008. DOI: 10.1117/12.794157.

[7] D. Camasão and D. Mantovani, "The mechanical characterization of blood vessels and their substitutes in the continuous quest for physiological-relevant performances. a critical review," *Materials Today Bio*, vol. 10, p. 100 106, 2021, ISSN: 2590-0064. DOI: https://doi.org/10.1016/j.mtbio.2021.100106. [Online]. Available: https://www.sciencedirect.com/science/article/pii/S2590006421000144.

[8] *Density and mass of each organ-tissue.* [Online]. Available: https://bionumbers.hms.harvard.edu/files/Density%20and%20mass%20of%20each%20organ-tissue.pdf#:~:text=URL%3A%20https%3A%2F%2Fbionumbers.hms.harvard.edu%2Ffiles%2FDensity%2520and%2520mass%2520of%2520each%2520organ.

[9] A. Kueh, S. Kenjeres, and N. Rusli, "Magnetic field effects on 3d blood flow patterns of straight and stenotic arteries," *Advanced Science Letters*, vol. 19, pp. 2690–2693, Sep. 2013. DOI: 10.1166/asl.2013.5018.

[10] E. Nader, S. Skinner, M. Romana, *et al.*, "Blood rheology: Key parameters, impact on blood flow, role in sickle cell disease and effects of exercise," en, *Front Physiol*, vol. 10, p. 1329, Oct. 2019.

[11] M. Klarhöfer, B. Csapo, C. Balassy, J. C. Szeles, and E. Moser, "High-resolution blood flow velocity measurements in the human finger," en, *Magn Reson Med*, vol. 45, no. 4, pp. 716–719, Apr. 2001.

[12] H. S. Ipek Y Enis and T. G. Sadikoglu, *Full factorial experimental design for mechanical properties of electrospun vascular grafts.* [Online]. Available: https://journals.sagepub.com/doi/pdf/10.1177/1528083717690614.

[13] X. Wang, V. Chan, and P. Corridon, "Acellular tissue-engineered vascular grafts from polymers: Methods, achievements, characterization, and challenges," *Polymers*, vol. 14, p. 4825, Nov. 2022. DOI: 10.3390/polym14224825.